Weierstraß-Institut
für Angewandte Analysis und Stochastik

im Forschungsverbund Berlin e.V.

Preprint ISSN 0946 – 8633

Transient Numerical Study of Temperature Gradients During Sublimation Growth of SiC: Dependence on Apparatus Design

Jürgen Geiser[1], Olaf Klein[1], and Peter Philip[2]

submitted: 12th December 2005

[1] Weierstrass Institute
for Applied Analysis
and Stochastics
Mohrenstrasse 39
D-10117 Berlin
Germany
E-Mail: geiser@wias-berlin.de
klein@wias-berlin.de

[2] Institute for Mathematics
and its Applications (IMA)
University of Minnesota
400 Lind Hall
207 Church Street S.E.
Minneapolis, MN 55455-0436
USA
E-Mail: philip@ima.umn.edu

No. 1080
Berlin 2005

2000 *Mathematics Subject Classification.* 80A20 80M25 76R50 65Z05 35K55.

Key words and phrases. Numerical simulation. SiC single crystal. Physical vapor transport. Heat transfer. Temperature gradients. Nonlinear parabolic PDE's.

2003 *Physics Abstract Classifications.* 02.60.Cb 81.10.Bk 44.05.+e 47.27.Te.

This work has been supported by the DFG Research Center MATHEON – "Mathematics for key technologies" (FZT 86) in Berlin and by the Institute for Mathematics and its Applications (IMA) in Minneapolis.

Edited by
Weierstraß-Institut für Angewandte Analysis und Stochastik (WIAS)
Mohrenstraße 39
10117 Berlin
Germany

Fax: + 49 30 2044975
E-Mail: preprint@wias-berlin.de
World Wide Web: http://www.wias-berlin.de/

Abstract

Using a transient mathematical heat transfer model including heat conduction, radiation, and radio frequency (RF) induction heating, we numerically investigate the time evolution of temperature gradients in axisymmetric growth apparatus during sublimation growth of silicon carbide (SiC) bulk single crystals by physical vapor transport (PVT) (modified Lely method). Temperature gradients on the growing crystal's surface can cause defects. Here, the evolution of these gradients is studied numerically during the heating process, varying the apparatus design, namely the amount of the source powder charge as well as the size of the upper blind hole used for cooling of the seed. Our results show that a smaller upper blind hole can reduce the temperature gradients on the surface of the seed crystal without reducing the surface temperature itself.

1 Introduction

Silicon carbide (SiC) is a wide-bandgap semiconductor used in high-power and high-frequency industrial applications: SiC serves as substrate material for electronic and optoelectronic devices such as MOSFETs, thyristors, blue lasers, and sensors (see [1] for a recent account of advances in SiC devices). Its chemical and thermal stability make SiC an attractive material to be used in high-temperature applications as well as in intensive-radiation environments. For an economically viable industrial use of SiC, growth techniques for large-diameter, low-defect SiC boules must be available. Recent years have seen steady improvement (see [2]) of size and quality of SiC single crystals grown by sublimation via *physical vapor transport* (PVT, also known as modified Lely method, see e.g. [3, 4]). However, many problems remain, warranting further research.

Typically, modern PVT growth systems consist of an induction-heated graphite crucible containing polycrystalline SiC source powder and a single-crystalline SiC seed (see Fig. 1). The source powder is placed in the hot zone of the growth apparatus, whereas the seed crystal is cooled by means of a blind hole, establishing a temperature difference between source and seed. As the SiC source is kept at a higher temperature than the cooled SiC seed, sublimation is encouraged at the source and crystallization is encouraged at the seed, causing the partial pressures of Si, Si_2C, and SiC_2 to be higher in the neighborhood of the source and lower in the neighborhood of the seed. As the system tries to equalize the partial pressures, source material is transported to the seed which grows into the reaction chamber.

Controlling the temperature distribution in the growth apparatus is essential to achieve low-defect growth of large SiC bulk single crystals. Experimental evidence shows that growth on the seed crystal can already occur during the heating phase [6], and experimental evidence also indicates that reducing temperature gradients

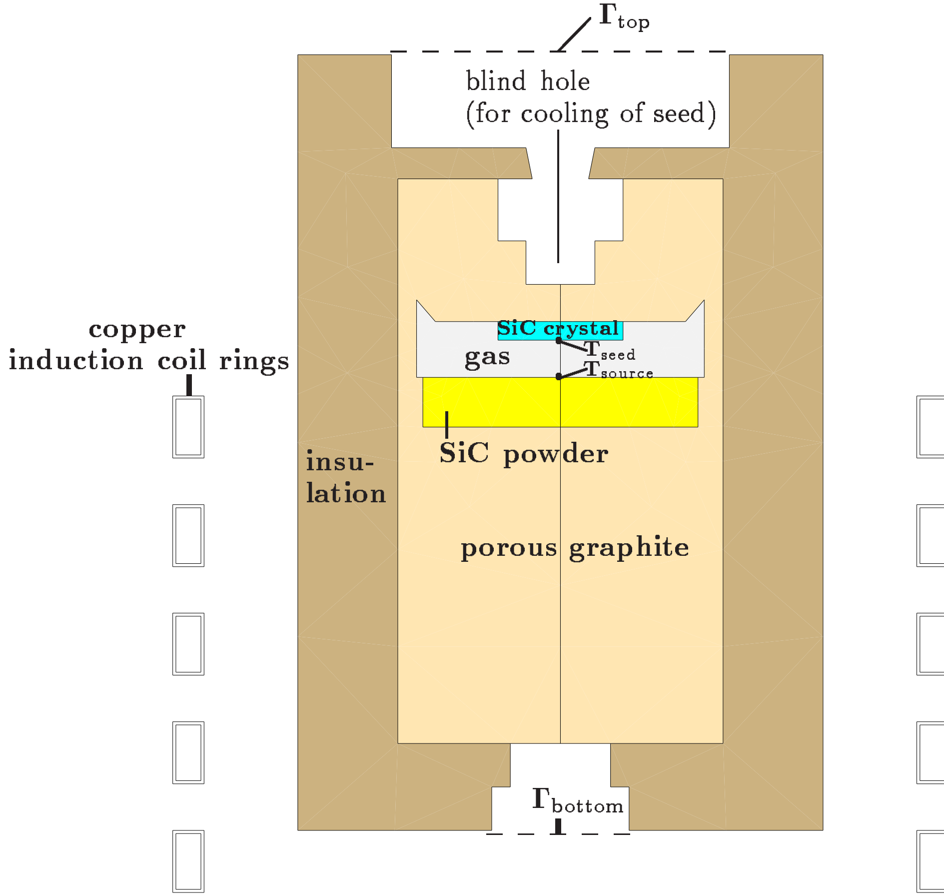

Figure 1: Setup of growth apparatus according to [5, Fig. 2].

(and resulting thermal stresses) on the surface of the seed crystal reduces the defect rate in the as-grown crystal [7, 8, 9]. However, owing to the high temperatures, experimental verification of the correlation between the design of the growth apparatus and the temperature distribution inside the growth chamber is extremely difficult and costly. In consequence, the development of numerical models and software and their application to PVT growth of SiC crystals has been an active field of research in recent years, see, e.g., [10, 11, 12, 13, 14] and references therein. While temperature fields in SiC growth systems and their dependence on PVT apparatus design has been the subject of many, both transient and stationary, numerical studies (including the above-quoted papers), the authors are not aware of a transient numerical investigation of the temperature gradient evolution including the heating stage, even though reducing temperature gradients in the initial growth stages is conducive to reducing crystal defects. It is the goal of the present paper to numerically simulate the evolution of the temperature field during the heating phase, assessing how varying the size of the upper blind hole and the size of the source powder charge can be used to reduce the temperature gradients.

The paper is organized as follows: In Sec. 2, we describe the mathematical model for

the heat transfer and for the induction heating. The employed numerical methods and the implementation tools are covered in Sec. 3. We present our numerical experiments in Sec. 4, where the general setting is detailed in 4.1, and numerical results analyzing the effect of the size of the upper blind hole as well as the amount of the source powder on the evolution of the temperature gradients on the surface of the SiC seed crystal are reported on and discussed in 4.2.

2 Modeling of Heat Transfer and Induction Heating

The numerical results of Sec. 4 below are based on our previously published model of transient heat transport in induction-heated PVT growth systems (see [15, 12] and references therein). For the convenience of the reader, we briefly recall the scope and assumptions of the model as well as the main governing equations, interface, and boundary conditions. The heat transport model includes conduction through solid materials as well as through the gas phase as described by the transient heat equations

$$\rho_m\,\partial_t\,\mathrm{e}_m + \operatorname{div}\vec{q}_m = f_m, \tag{1a}$$

$$\vec{q}_m = -\kappa_m(T)\,\nabla T \quad \text{in } \Omega_m, \tag{1b}$$

where the index m refers to a material that can be either the gas phase or a solid component of the growth apparatus, ρ_m denotes mass density, t denotes time, e_m denotes internal energy, $\vec{q}_m$ denotes heat flux, f_m denotes power density (per volume) caused in conducting materials due to induction heating, κ_m denotes thermal conductivity, T denotes absolute temperature, and Ω_m is the domain of material m.

It is assumed that the gas phase is made up solely of argon, which is a reasonable assumption for simulations of the temperature distribution [16, Sec. 5]. Then, the internal energy in the gas phase takes the form

$$\mathrm{e}_{\mathrm{gas}}(T) = 3\,R\,T/(2\,M_{\mathrm{Ar}}), \tag{2a}$$

R denoting the gas constant, and M_{Ar} denoting the mass density and molecular mass of argon, respectively. The internal energy of the solid material m_i is given by

$$\mathrm{e}_{m_i}(T) = \int_{T_0}^{T} c_{m_i}(S)\,\mathrm{d}S\,, \tag{2b}$$

where c denotes specific heat, and T_0 is a reference temperature. The temperature is assumed to be continuous throughout the apparatus. To formulate the interface conditions for the heat flux, let β and β' denote different solid components of the growth apparatus. The normal heat flux is assumed to be continuous on an interface $\gamma_{\beta,\beta'}$ between two solid materials β and β', i.e. the interface condition is given by (3a). If the solid material β is the semi-transparent SiC single crystal or on an interface

$\gamma_{\beta',\text{gas}}$ between the solid material β' and the gas phase, one needs to account for radiosity R and for irradiation J, resulting in interface conditions (3b) and (3c), respectively.

$$\vec{q}^{\,[\beta]} \bullet \vec{n}^{\,[\beta]} = \vec{q}^{\,[\beta']} \bullet \vec{n}^{\,[\beta]} \quad \text{on } \gamma_{\beta,\beta'}, \tag{3a}$$

$$\vec{q}^{\,[\beta]} \bullet \vec{n}^{\,[\beta]} - R + J = \vec{q}^{\,[\beta']} \bullet \vec{n}^{\,[\beta]} \quad \text{on } \gamma_{\beta,\beta'}, \tag{3b}$$

$$\vec{q}_{\text{gas}} \bullet \vec{n}_{\text{gas}} - R + J = \vec{q}^{\,[\beta]} \bullet \vec{n}_{\text{gas}} \quad \text{on } \gamma_{\beta,\text{gas}}, \tag{3c}$$

where $\vec{n}^{\,[\beta]}$ is the outer unit normal vector to the solid material β, and $\vec{n}_{\text{gas}}$ is the outer unit normal vector to the gas phase. The radiative quantities R and J are modeled using the net radiation method for diffuse-gray radiation as described in [12, Sec. 2.5], where a band approximation model is used to account for the semi-transparency of the SiC single crystal. The growth apparatus is considered in a black body environment (e.g. a large isothermal room) radiating at room temperature T_{room}, such that outer boundaries emit according to the Stefan-Boltzmann law:

$$\vec{q}^{\,[\beta]} \bullet \vec{n}^{\,[\beta]} = \sigma \epsilon^{[\beta]} (T^4 - T_{\text{room}}^4), \tag{4}$$

where $\sigma = 5.6696 \cdot 10^{-8} \frac{\text{W}}{\text{m}^2\text{K}^4}$ denotes the Boltzmann radiation constant, and $\epsilon^{[\beta]}$ denotes the (temperature-dependent) emissivity of the surface. On outer boundaries receiving radiation from other parts of the apparatus, i.e. on the surfaces of the upper and lower blind hole, the situation is more complicated. On such boundaries, as in (3b) and (3c), one has to account for radiosity R and irradiation J, leading to the boundary condition

$$\vec{q}^{[\beta]} \bullet \vec{n}^{[\beta]} - R + J = 0, \tag{5}$$

where, as before, the modeling of R and J is as described in [12, Sec. 2.5]. For the two blind holes, we use black body phantom closures (denoted by Γ_{top} and Γ_{bottom} in Fig. 1) which emit radiation at T_{room}. We thereby allow for radiative interactions between the open cavities and the ambient environment, including reflections at the cavity surfaces.

Induction heating causes eddy currents in the conducting materials of the growth apparatus, resulting in the heat sources f_m of (1a) due to the Joule effect. Assuming axisymmetry of all components of the growth system as well as of all relevant physical quantities, and, furthermore, assuming sinusoidal time dependence of the imposed alternating voltage, the heat sources are computed via an axisymmetric complex-valued magnetic scalar potential that is determined as the solution of an elliptic partial differential equation (see [12, Sec. 2.6]). To prescribe the total heating power, we follow [17, Sec. II], ensuring that the total current is the same in each coil ring. The distribution of the heat sources is redetermined in each time step of the transient problem for the temperature evolution to account for temperature dependence of the electrical conductivity.

All simulations presented in this article are performed for an idealized growth apparatus, treating all solid materials as homogeneous and pure, neglecting effects such as the sintering of the SiC source powder, changes in the porosity of the graphite, and Si accumulation in the insulation.

3 Numerical Methods and Implementation

For the numerical computations presented in Sec. 4.2 below, i.e. for the stationary simulations of the magnetic scalar potential as well as for the transient temperature simulations, a finite volume method is used for the spatial discretizations of the nonlinear partial differential equations that arise from the model described in Sec. 2 above. An implicit Euler scheme provides the time discretization of the temperature evolution equation; only emissivity terms are evaluated explicitly, i.e. using the temperature at the previous time step. The used scheme, including the discretization of nonlocal terms stemming from the modeling of diffuse-gray radiation, was previously described in [15, 18]. The convergence of the scheme has been verified numerically for stationary cases in [19, 20].

The finite volume discretization of the nonlocal radiation terms involves the calculation of visibility and view factors. The method used is based on [21] and is described in [16, Sec. 4].

The discrete scheme was implemented as part of our software *WIAS-HiTNIHS*[1] which is based on the program package *pdelib* [22]. In particular, *pdelib* uses the grid generator *Triangle* [23] to produce constrained Delaunay triangulations of the domains, and it uses the sparse matrix solver *PARDISO* [24, 25] to solve the linear system arising from the linearization of the finite volume scheme via Newton's method.

4 Numerical Experiments

4.1 General Setting

All numerical simulations presented in the following were performed for the growth system [5, Fig. 2] displayed in Fig. 1, consisting of a container having a radius of 8.4 cm and a height of 25 cm placed inside of 5 hollow rectangular-shaped copper induction rings. Using cylindrical coordinates (r, z), the upper rim of the induction coil is located at $z = 14$ cm, and its lower rim is located at $z = -2.0$ cm, i.e. 2 cm lower than the lower rim of the rest of the apparatus (see Fig. 1). The geometric proportions of the coil rings are provided in Fig. 2.

The material data used for the following numerical experiments are precisely the data provided in the appendices of [16], [26], and [27], respectively. The angular frequency used for the induction heating is $\omega = 2\pi f$, where $f = 10$ kHz. The

[1]**H**igh **T**emperature **N**umerical **I**nduction **H**eating **S**imulator; pronunciation: ~hit-nice.

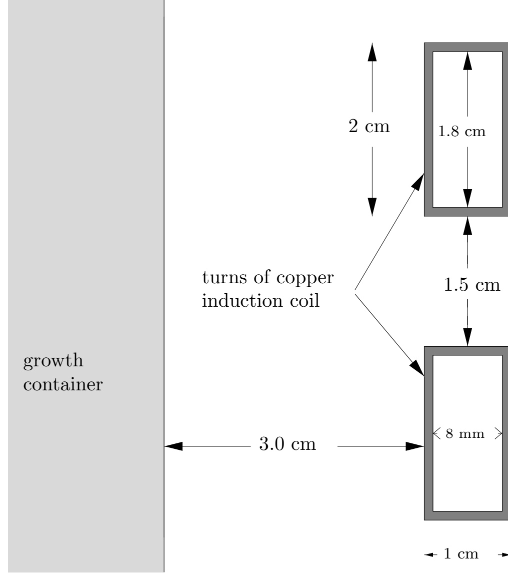

Figure 2: Geometric proportions of induction coil rings.

average total power P is prescribed according to the following linear ramp:

$$P(t) := \begin{cases} P_{\min} & \text{for } t \leq t_0, \\ P_{\min} + \frac{(t-t_0)(P_{\max}-P_{\min})}{t_1-t_0} & \text{for } t_0 \leq t \leq t_1, \\ P_{\max} & \text{for } t_1 \leq t, \end{cases} \tag{6}$$

where $t_0 = 0.5$ h, $t_1 = 3.0$ h, $P_{\min} = 2$ kW, and $P_{\max} = 7$ kW.

Each simulation starts at $T_{\text{room}} = 293$ K.

4.2 Transient Numerical Investigation of the Temperature Gradient

We conduct four numerical experiments, varying the amount of the source powder and the size of the upper blind hole. We consider two different amounts of source powder, where the larger amount is 5 times the smaller amount. We employ the abbreviations powder=1 and powder=5 to indicate the use of the small and large amount of source powder, respectively. We consider two different sizes for the upper blind hole, the situation with the smaller hole being referred to as hole=0, and the situation with the larger hole being referred to as hole=1. The resulting different apparatus designs used in the four experiments are depicted in Fig. 3: We use powder=1, hole=1 in Experiment (a); powder=5, hole=1 in Experiment (b); powder=1, hole=0 in Experiment (c); and powder=5, hole=0 in Experiment (d).

As described earlier, controlling the temperature gradient on the surface of the SiC

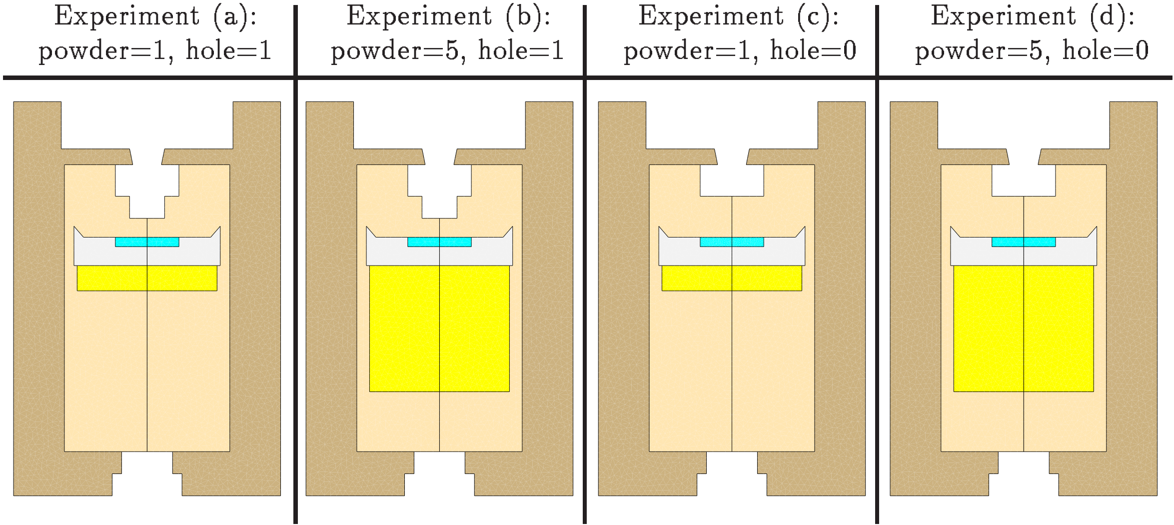

Figure 3: Apparatus designs for Experiments (a) – (d).

single crystal seed is of particular importance in order to avoid crystal defects in the as-grown crystal. We, therefore, pay special attention to the evolution of the temperature gradient on the seed's surface in the following analysis of the numerical results. In each of the considered apparatus designs, the seed's surface Σ is the set

$$\Sigma := \big\{(r, \theta, z) : 0 \le r \le 2\,\mathrm{cm},\ z = 15.8\,\mathrm{cm}\big\}, \tag{7}$$

where, here and in the following, (r, θ, z) denote cylindrical coordinates. Due to cylindrical symmetry, the temperature gradient is completely described by its radial and by its vertical component: $\nabla T = (\partial_r T, \partial_z T)$. As the material properties are discontinuous across Σ (the gas phase being below and the seed crystal being above Σ), ∇T can be discontinuous across Σ as well. Thus, for $(r, z) \in \Sigma$, we compute two values for ∇T, namely one value for the crystal side, denoted ∇T_{seed}, and one value for the gas side, denoted ∇T_{gas}. More precisely, for $(r, z) \in \Sigma$, we compute the following approximations:

$$\nabla T_{\mathrm{seed}}(r, z) := \left(\frac{T(r + 0.5\,\mathrm{mm}, z) - T(r - 0.5\,\mathrm{mm}, z)}{1.0\,\mathrm{mm}}, \frac{T(r, z + 0.5\,\mathrm{mm}) - T(r, z)}{0.5\,\mathrm{mm}}\right),$$

$$\nabla T_{\mathrm{gas}}(r, z) := \left(\frac{T(r + 0.5\,\mathrm{mm}, z) - T(r - 0.5\,\mathrm{mm}, z)}{1.0\,\mathrm{mm}}, \frac{T(r, z - 0.5\,\mathrm{mm}) - T(r, z)}{-0.5\,\mathrm{mm}}\right),$$

with the modifications

$$\partial_r T(0, z) := \big(T(0.5\,\mathrm{mm}, z) - T(0, z)\big)/0.5\,\mathrm{mm},$$
$$\partial_r T(2\,\mathrm{cm}, z) := \big(T(2.0\,\mathrm{cm}, z) - T(1.95\,\mathrm{cm}, z)\big)/0.5\,\mathrm{mm}.$$

On each triangle of the mesh, the values for T are computed via affine interpolation according to the values at the vertices given by the discrete solution to the finite

Exp. time [s]	(a) 5000	(b) 5000	(c) 5000	(d) 5000
$\partial_r T_{\mathsf{seed}}(0, 15.8\,\mathrm{cm})[\mathrm{K/m}]$	6.43	7.77	7.36	8.20
$\partial_z T_{\mathsf{seed}}(0, 15.8\,\mathrm{cm})[\mathrm{K/m}]$	-9.39	-10.0	-8.65	-10.9
$\partial_r T_{\mathsf{seed}}(1.9\,\mathrm{cm}, 15.8\,\mathrm{cm})[\mathrm{K/m}]$	44.1	47.9	44.9	50.3
$\partial_z T_{\mathsf{seed}}(1.9\,\mathrm{cm}, 15.8\,\mathrm{cm})[\mathrm{K/m}]$	15.0	13.5	12.4	11.5
Exp. time [s]	(a) 10000	(b) 10000	(c) 10000	(d) 10000
$\partial_r T_{\mathsf{seed}}(0, 15.8\,\mathrm{cm})[\mathrm{K/m}]$	17.4	19.6	13.3	14.2
$\partial_z T_{\mathsf{seed}}(0, 15.8\,\mathrm{cm})[\mathrm{K/m}]$	-62.8	-48.9	-34.7	-36.5
$\partial_r T_{\mathsf{seed}}(1.9\,\mathrm{cm}, 15.8\,\mathrm{cm})[\mathrm{K/m}]$	98.3	101	82.2	87.2
$\partial_z T_{\mathsf{seed}}(1.9\,\mathrm{cm}, 15.8\,\mathrm{cm})[\mathrm{K/m}]$	7.45	5.36	-3.50	-5.94
Exp. time [s]	(a) 20000	(b) 20000	(c) 20000	(d) 20000
$\partial_r T_{\mathsf{seed}}(0, 15.8\,\mathrm{cm})[\mathrm{K/m}]$	21.2	23.2	14.5	15.1
$\partial_z T_{\mathsf{seed}}(0, 15.8\,\mathrm{cm})[\mathrm{K/m}]$	-97.0	-72.9	-54.1	-53.7
$\partial_r T_{\mathsf{seed}}(1.9\,\mathrm{cm}, 15.8\,\mathrm{cm})[\mathrm{K/m}]$	122	122	97.5	99.9
$\partial_z T_{\mathsf{seed}}(1.9\,\mathrm{cm}, 15.8\,\mathrm{cm})[\mathrm{K/m}]$	-9.62	-10.9	-23.5	-25.8

Table 1: Three temporal snapshots of the values of the temperature gradient $\nabla T_{\mathsf{seed}} = (\partial_r T_{\mathsf{seed}}, \partial_z T_{\mathsf{seed}})$ inside the seed crystal, taken at the surface at $(r, z) = (0, 15.8\,\mathrm{cm})$ and at $(r, z) = (1.9\,\mathrm{cm}, 15.8\,\mathrm{cm})$ for Experiments (a) – (d).

volume scheme. In a neighborhood of the seed crystal's surface, the grid was chosen sufficiently fine such that the diameter of each triangle was less than 0.5 mm. Figures 4 and 5 depict the time evolution of $\nabla T_{\mathsf{seed}}(r, z)$ for $(r, z) = (0, 15.8\,\mathrm{cm})$ and for $(r, z) = (1.9\,\mathrm{cm}, 15.8\,\mathrm{cm})$, respectively, where the radial component is shown in the first row, the vertical component is shown in the second row, and the angle ϕ_{seed} between ∇T_{seed} and the $r = 0$ axis is shown in the third row. Moreover, the precise values for three temporal snapshots of $\nabla T_{\mathsf{seed}}(r, z)$ at $(r, z) = (0, 15.8\,\mathrm{cm})$ and at $(r, z) = (1.9\,\mathrm{cm}, 15.8\,\mathrm{cm})$ are compiled in Table 1. Figure 6 depicts the evolution of the L^2-norm of the radial temperature gradient on the seed's surface, i.e. of

$$\|\partial_r T\|_{2,\Sigma} = \sqrt{\int_{\Sigma} |\partial_r T|^2} = \sqrt{2\,\pi \int_0^{2\,\mathrm{cm}} r\,|\partial_r T(r, 15.8\,\mathrm{cm})|^2\,\mathrm{d}r}\,. \tag{8}$$

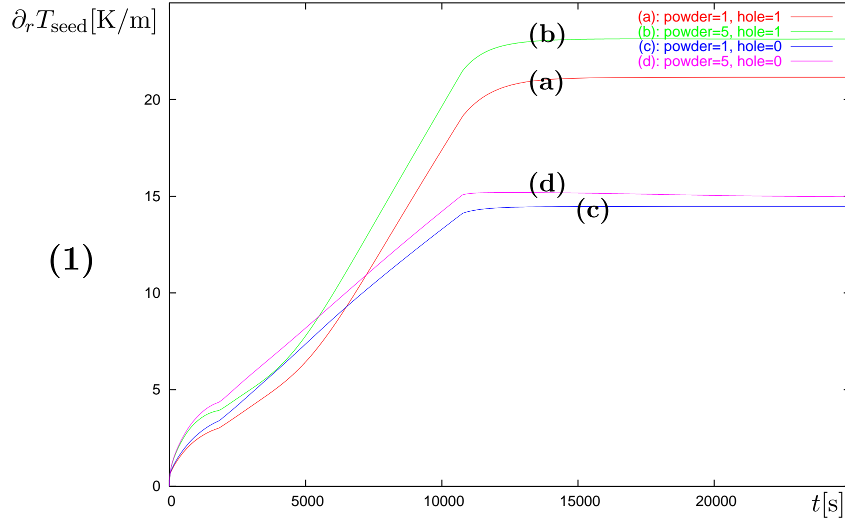

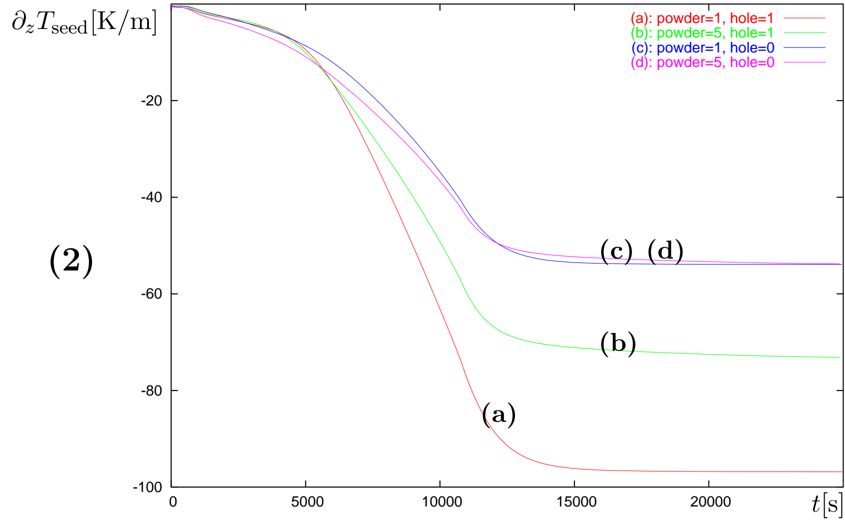

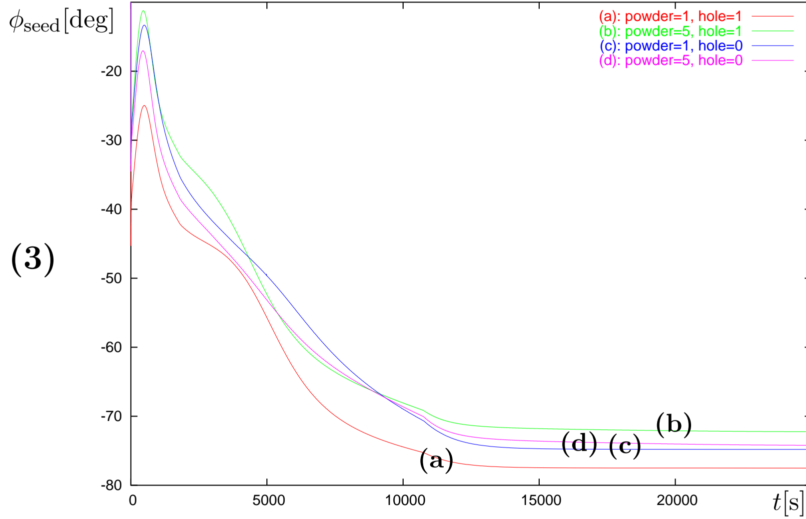

Figure 4: Evolution of the temperature gradient $\nabla T_{\text{seed}} = (\partial_r T_{\text{seed}}, \partial_z T_{\text{seed}})$ inside the seed crystal, taken at the surface at $(r, z) = (0, 15.8\,\text{cm})$ for Experiments (a) – (d); ϕ_{seed} is the angle between ∇T_{seed} and the $r = 0$ axis.

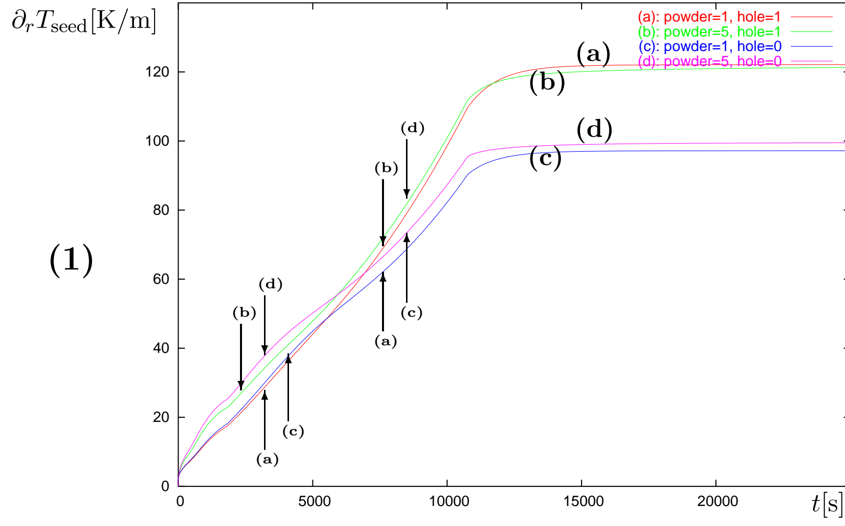

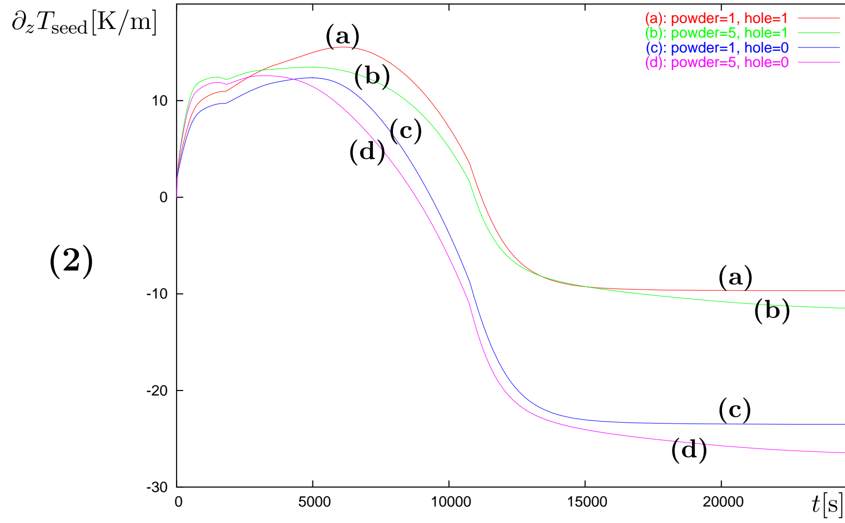

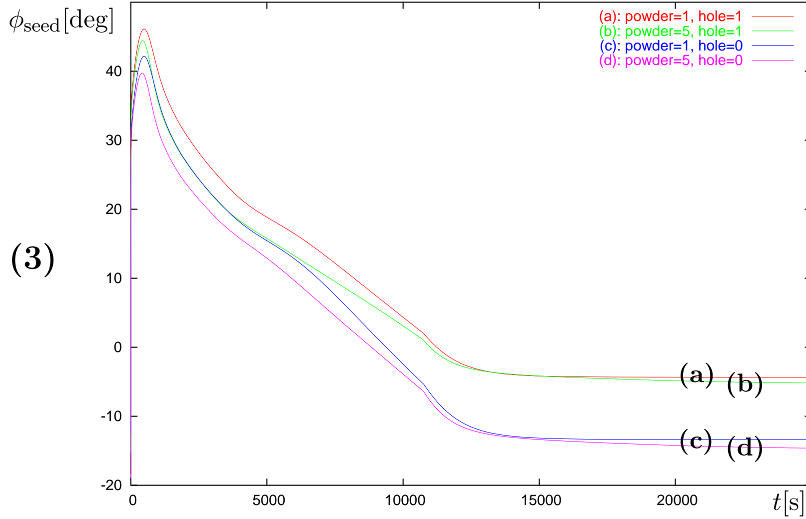

Figure 5: Evolution of the temperature gradient $\nabla T_{\text{seed}} = (\partial_r T_{\text{seed}}, \partial_z T_{\text{seed}})$ inside the seed crystal, taken at the surface at $(r, z) = (1.9\,\text{cm}, 15.8\,\text{cm})$ for Experiments (a) – (d); ϕ_{seed} is the angle between ∇T_{seed} and the $r = 0$ axis.

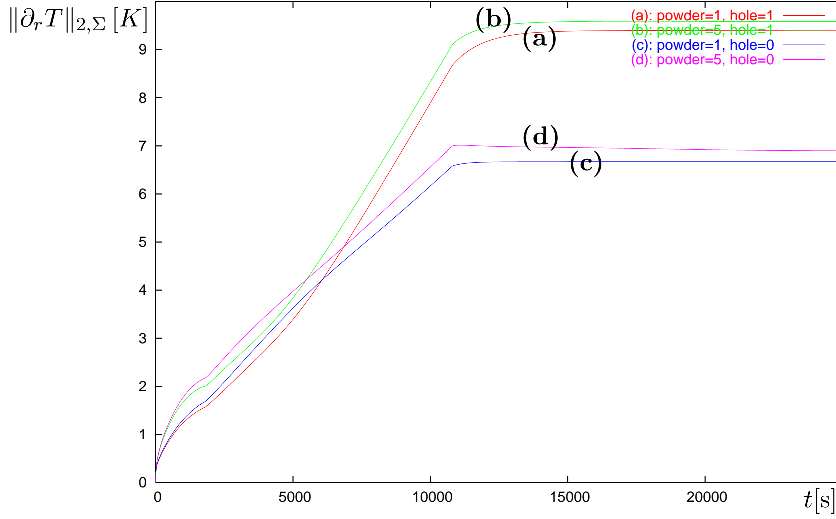

Figure 6: Evolution of the L^2-norm of the radial temperature gradient $\partial_r T$ on the seed's surface Σ (see (8)) for Experiments (a) – (d).

Figure 7 provides information on the temperature field evolution in the gas phase between SiC source and seed, namely the evolution of $T_{\text{source}} - T_{\text{seed}} = T(0, 14.6\,\text{cm}) - T(0, 15.8\,\text{cm})$ in Row (1) (cf. Fig. 1) and of ∇T_{gas} at $(r, z) = (0, 15.8\,\text{cm})$ in Rows (2) and (3): The vertical component $\partial_z T_{\text{gas}}$ is shown in Row (2), and the angle ϕ_{gas} between ∇T_{gas} and the $r = 0$ axis is shown in Row (3). Finally, the evolution of $T_{\text{seed}} = T(0, 15.8\,\text{cm})$ is portrayed in Fig. 8.

We start by discussing some general patterns of heat field evolution present in each of the four experiments, and we then proceed to analyze the differences caused by the design modifications. In each experiment, the heat sources are mainly concentrated close to the vertical surface of the graphite crucible in the lower part of the apparatus, due to the low position of the induction coil rings (see Fig. 1). During the initial phase of the heating process, i.e. while the apparatus is still at low temperatures and radiation has little effect, the thermal conductivities of the SiC source powder and of the gas phase are very low as compared to those of the graphite and of the SiC seed. Thus, originating in the lower graphite part of the apparatus, upward flowing heat mainly travels *around* the SiC powder and the gas phase, reaching the SiC seed crystal from the upper right-hand graphite region above the SiC seed. This situation is reflected in Fig. 5, where both the radial and vertical component of $\nabla T_{\text{seed}}(1.9\,\text{cm}, 15.8\,\text{cm})$ are shown to be increasing during the first 4000 seconds, such that ∇T_{seed} is initially pointing upward and to the right (see Fig. 5(3)). The behavior of the radial gradient $\partial_r T_{\text{seed}}$ at $(0, 15.8\,\text{cm})$ is similar (Fig. 4(1)), but the vertical gradient $\partial_z T_{\text{seed}}$ at $(0, 15.8\,\text{cm})$ is always negative. This can be explained by the insulating effect of the inner gas phase in combination with the cooling effect of the upper blind hole. In Fig. 7, the initial phase is characterized by the temperature being higher at the seed than at the source

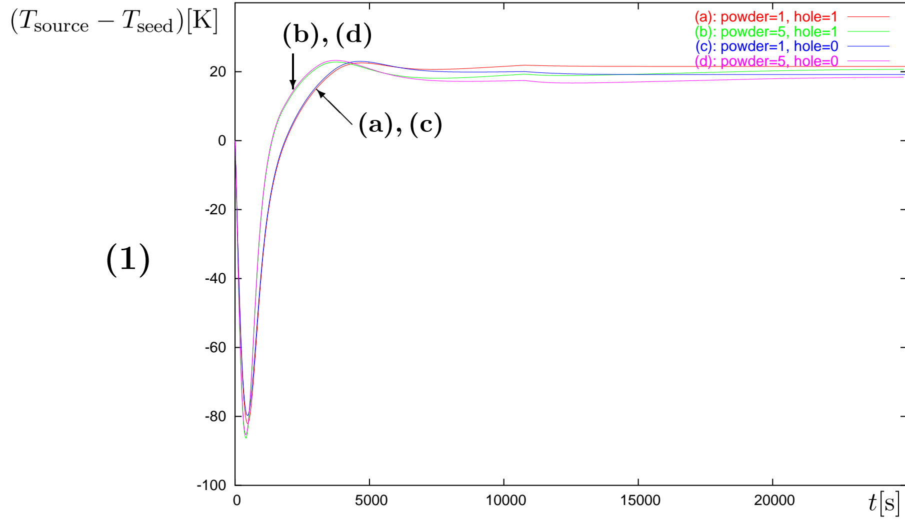

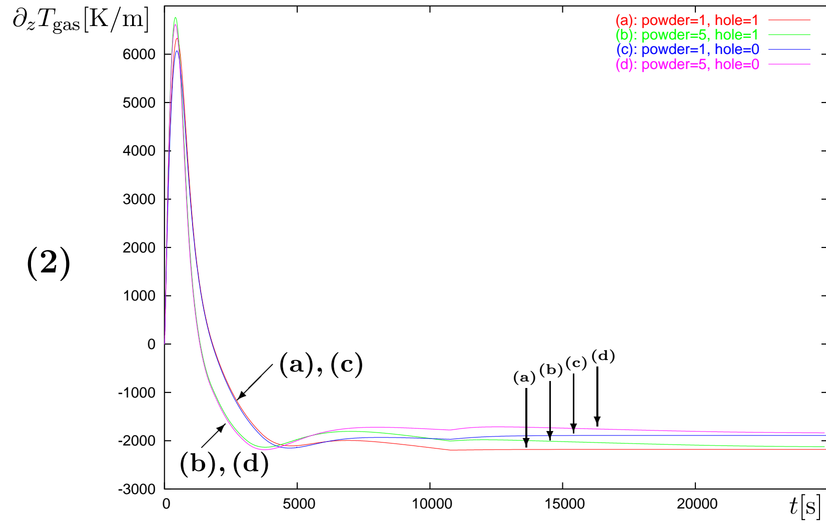

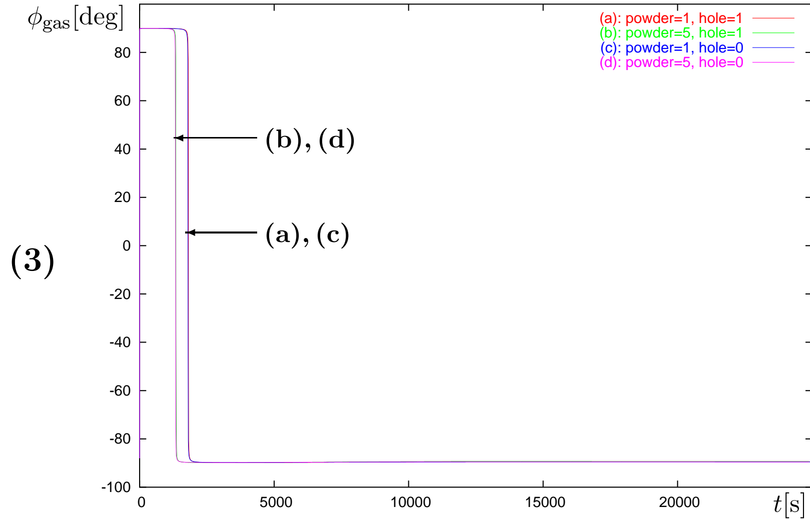

Figure 7: Evolution of $T_{\text{source}} - T_{\text{seed}}$ and of the vertical temperature gradient $\partial_z T_{\text{gas}}$ inside the gas phase, taken at the seed's surface at $(r, z) = (0, 15.8\,\text{cm})$ for Experiments (a) – (d); ϕ_{gas} is the angle between ∇T_{gas} and the $r = 0$ axis.

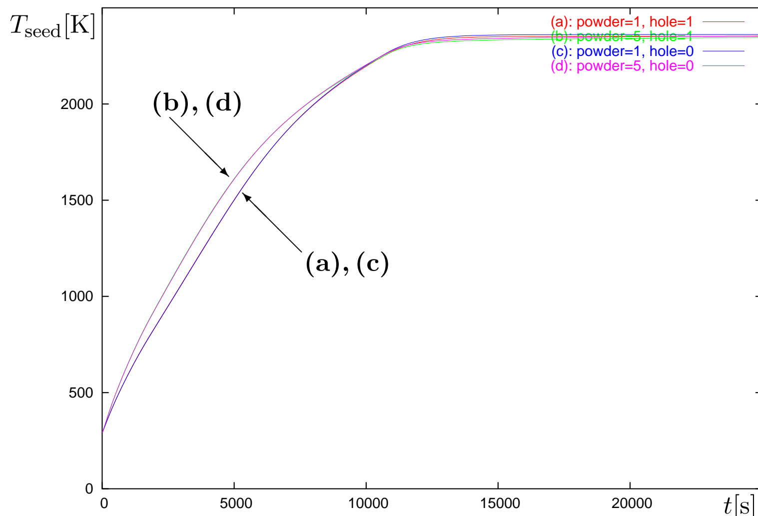

Figure 8: Evolution of $T_{\rm seed}$, i.e. of the temperature at $(r, z) = (0, 15.8\,\text{cm})$, for Experiments (a) – (d).

(Fig. 7(1)) and a large, upward-pointing temperature gradient $\nabla T_{\rm gas}$ (Fig. 7(1),(2)).

As the temperature in the apparatus continuous to increase, so does the radial gradient on the seed's surface Σ (Figures 4(1), 5(1), 6, Table 1), as the heat continuous to flow from the outside to the inside of the apparatus. However, as the radiative heat transfer through the gas phase and through the SiC powder becomes more effective, both domains become less thermally insulating, such that more and more heat reaches Σ from the gas phase, resulting in the decreasing vertical temperature gradients in Figures 4(2), 5(2), and 7(2). In particular, after some 2000 s, $T_{\rm source} - T_{\rm seed}$ becomes positive (Fig. 7(1)), $\partial_z T_{\rm gas}$ becomes negative (Fig. 7(2)), and $\nabla T_{\rm gas}$ turns from pointing from seed to source to pointing from source to seed (Fig. 7(3)). Thus, the source becomes warmer than the seed as is required for the growth process.

While the seed temperatures reached at the end of the heating process (see Fig. 8) as well as the qualitative evolutions of the considered temperature gradients are quite close for each of the apparatus designs (a) – (d) as discussed above, we now come to important quantitative differences in the temperature gradient evolutions. First, we consider $\nabla T_{\rm seed}$ on Σ (Figures 4 and 5, Table 1), i.e. the temperature gradient inside the seed crystal close to the surface where growth is supposed to occur. It is reiterated that the goal is to keep $\nabla T_{\rm seed}$ low to avoid defects due to thermal stress during growth. We find from Fig. 8 that the temperature at the seed's surface reaches 1500 K after approximately 4000 s for Experiments (b), (d); and after approximately 5000 s for Experiments (a), (c). Initial growth is not expected to occur below this temperature, and, therefore, we focus on $t > 4000\,\text{s}$ in the following discussion.

Comparing Figures 4(1), 4(2), 5(1), 5(2), and evaluating the upper part of Table 1, one finds that, at t=5000 s, the radial gradient on Σ far from the axis

($|\partial_r T_{\text{seed}}(1.9\,\text{cm}, 15.8\,\text{cm})|$, Fig. 5(1)) has the largest absolute values, namely 44-51 K/m, while $|\partial_r T_{\text{seed}}(0, 15.8\,\text{cm})|$, $|\partial_z T_{\text{seed}}(0, 15.8\,\text{cm})|$, $|\partial_z T_{\text{seed}}(1.9\,\text{cm}, 15.8\,\text{cm})|$ are all below 15 K/m. At t=5000 s, the $|\partial_r T_{\text{seed}}(1.9\,\text{cm}, 15.8\,\text{cm})|$ in increasing order by experiment are (a), (c), (b), (d) with some 6 K/m difference between (a) (powder=1, hole=1) and (d) (powder=5, hole=0). However, the order has changed to (c), (d), (a), (b) by t=7500 s; and to (c), (d), (b), (a) by t=12500 s. At this time, the values for $|\partial_r T_{\text{seed}}(1.9\,\text{cm}, 15.8\,\text{cm})|$ have increased to 90-120 K/m. For the experiments with the smaller hole, (c), (d), the value is some 30 K/m lower than for the experiments with the larger hole (a), (b). The size of the powder charge has a much smaller influence on the size of the gradient. That, at least at higher temperatures, the size of ∇T_{seed} on Σ depends more on the size of the upper blind hole than on the size of the powder charge, can also be observed in Figures 4(1) and 4(2) as well as in Table 1. In each case, the gradients are found to be smaller for the smaller blind hole, which is also confirmed in Fig. 6, where the radial gradient is integrated over the entire surface Σ. The smallest value is, again, found for (c) (powder=1, hole=0). Since the upper blind hole is in much closer proximity to the seed crystal than to the source powder charge, it is not unexpected that its size has a stronger effect on the temperature gradients at Σ. The dominance of $|\partial_r T_{\text{seed}}(1.9\,\text{cm}, 15.8\,\text{cm})|$ over the other three values remains true throughout the heating process. However, note from Fig. 4(2) and from the lower part of Table 1 that, in Exp. (a) (powder=1, hole=1), $|\partial_z T_{\text{seed}}(0, 15.8\,\text{cm})|$ comes close to 100 K/m for $t > 15000\,\text{s}$, thereby being significantly larger than for the other three experiments.

Summarizing the above findings, we note that, even though the dependence of the size of ∇T_{seed} at Σ on the hole size and on the amount of source powder changes during the heating process, for $t > 7500\,\text{s}$, ∇T_{seed} at Σ is consistently smaller for the hole=0 experiments (c), (d), with a slight advantage for (c), i.e. powder=1. As the size of ∇T_{seed} on Σ increases with temperature and time in each case, it is more important to keep ∇T_{seed} small for $t > 7500\,\text{s}$ than for $t < 7500\,\text{s}$. Moreover, we found that the maximal size of ∇T_{seed} on Σ is determined by $|\partial_r T_{\text{seed}}(1.9\,\text{cm}, 15.8\,\text{cm})|$. This is in agreement with the results of [7, 8], where the quality of as-grown crystals was found to be improved by reducing the radial temperature gradients. However, we also point out that the radial temperature gradient on Σ was always less than 130 K/m during all our simulations, and, thus, lower than the 200 K/m that resulted in good-quality crystals according to [7].

Finally, we remark that Figure 7 shows that the direction of the temperature gradient in the gas phase ∇T_{gas} on Σ turns some 500 s earlier in (b), (d) (for powder=5) as compared to (a), (c) (powder=1), so that the SiC source becomes warmer than the SiC seed. However, Figure 8 shows that, in (b), (d), T_{seed} reaches growth temperature earlier than in (a), (c). More importantly, Figures 7 and 8 show that $T_{\text{source}} - T_{\text{seed}}$ becomes positive in all cases before T_{seed} reaches 1500 K.

5 Conclusions

Based on a transient heat transfer model implemented in the software *WIAS-HiTNIHS*, the evolution of temperature fields was simulated for four different axisymmetric setups of PVT growth systems, varying the size of the upper blind hole and the amount of the source powder charge. The temperature gradients were monitored in the vicinity of the SiC seed crystal's surface, where they are closely related to the quality of the as-grown crystal. The temperature gradients in the seed were found to increase with time and temperature, their maximal size being determined by the radial gradients far from the symmetry axis. These gradients were some 30 K/m smaller for the smaller blind hole. The size of the gradients was found to depend much less on the size of the powder charge, but being slightly smaller for the smaller amount of source powder. The seed temperature reached at the end of the heating process did not vary significantly with the considered different designs. This fact is especially noteworthy in the light of [14], where temperature-constrained stationary numerical optimizations showed that low radial temperature gradients can be achieved by reducing the crystal's temperature. However, as the growth process requires one to keep the seed crystal above a certain temperature, adjusting the size of the upper blind hole can furnish a useful alternative for further reduction of the radial temperature gradients.

6 Acknowledgments

This work has been supported by the Institute for Mathematics and its Applications (IMA) in Minneapolis, by the DFG Research Center MATHEON – "Mathematics for key technologies" (FZT 86) in Berlin, and by Corning Incorporated, Corning, NY.

References

[1] Ch. 9–11, Vol. 457–460, Part II of Madar et al. [28].

[2] H.McD. Hobgood, M.F. Brady, M.R. Calus, J.R. Jenny, R.T. Leonard, D.P. Malta, St.G. Müller, A.R. Powell, V.F. Tsvetkov, R.C. Glass, C.H. Carter, Jr., Silicon carbide crystal and substrate technology: A survey of recent advances, Mater. Sci. Forum 457–460 (2004) 3–8, Proceedings of the 10th International Conference on Silicon Carbide and Related Materials, October 5–10, 2003, Lyon, France.

[3] Yu.M. Tairov, V.F. Tsvetkov, Investigation of growth processes of ingots of silicon carbide single crystals, J. Crystal Growth 43 (1978) 209–212.

[4] A.O. Konstantinov, Sublimation growth of SiC, pp. 170–203 in G.L. Harris (Ed.), Properties of Silicon Carbide, No. 13 in EMIS Datareview Series, Institution of Electrical Engineers, INSPEC, London, UK, 1995.

[5] M. Pons, M. Anikin, K. Chourou, J.M. Dedulle, R. Madar, E. Blanquet, A. Pisch, C. Bernard, P. Grosse, C. Faure, G. Basset, Y. Grange, State of the art in the modelling of SiC sublimation growth, Mater. Sci. Eng. B 61-62 (1999) 18–28.

[6] D. Schulz, M. Lechner, H.-J. Rost, D. Siche, J. Wollweber, On the early stages of sublimation growth of 4H-SiC using 8° off-oriented substrates, Mater. Sci. Forum 433–436 (2003) 17–20, Proceedings of 4th European Conference on Silicon Carbide and Related Materials, September 2–5, 2002, Linköping, Sweden.

[7] C.M. Balkas, A.A. Maltsev, M.D. Roth, V.D. Heydemann, M. Sharma, N.K. Yushin, Reduction of macrodefects in bulk sic single crystals, Mater. Sci. Forum 389–393 (2002) 59–62, Proceedings of the 9th International Conference on Silicon Carbide and Related Materials, October 27 – November 2, 2001, Tsukuba, Japan.

[8] S. Wang, E.M. Sanchez, A. Kopec, S. Poplawski, R. Ware, S. Holmes, C.M. Balkas, A.G. Timmerman, Growth of 3-inch diameter 6H-SiC single crystals by sublimation physical vapor transport, Mater. Sci. Forum 389–393 (2002) 35–38, Proceedings of the 9th International Conference on Silicon Carbide and Related Materials, October 27 – November 2, 2001, Tsukuba, Japan.

[9] S.I. Nishizawa, T. Kato, Y. Kitou, N. Oyanagi, F. Hirose, H. Yamaguchi, W. Bahng, K. Arai, High-quality SiC bulk single crystal growth based on simulation and experiment, Mater. Sci. Forum 457–460 (2004) 29–34.

[10] S.Yu. Karpov, A.V. Kulik, I.A. Zhmakin, Yu.N. Makarov, E.N. Mokhov, M.G. Ramm, M.S. Ramm, A.D. Roenkov, Yu.A. Vodakov, Analysis of sublimation growth of bulk SiC crystals in tantalum container, J. Crystal Growth 211 (2000) 347–351.

[11] R. Ma, H. Zhang, V. Prasad, M. Dudley, Growth kinetics and thermal stress in the sublimation growth of silicon carbide, Crystal Growth & Design 2 (3) (2002) 213–220.

[12] O. Klein, P. Philip, J. Sprekels, Modeling and simulation of sublimation growth of sic bulk single crystals, Interfaces and Free Boundaries 6 (2004) 295–314.

[13] J. Meziere, M. Pons, L. Di Cioccio, E. Blanquet, P. Ferret, J.M. Dedulle, F. Baillet, E. Pernot, M. Anikin, R. Madar, T. Billon, Contribution of numerical simulation to silicon carbide bulk growth and epitaxy, J. Phys.-Condes. Matter 16 (2004) S1579–S1595.

[14] C. Meyer, P. Philip, Optimizing the temperature profile during sublimation growth of sic single crystals: Control of heating power, frequency, and coil position, Crystal Growth & Design 5 (3) (2005) 1145–1156.

[15] P. Philip, Transient numerical simulation of sublimation growth of SiC bulk single crystals. Modeling, finite volume method, results, Ph.D. thesis, Department of Mathematics, Humboldt University of Berlin, Germany, 2003. Report No. 22, Weierstrass Institute for Applied Analysis and Stochastics (WIAS), Berlin. Available at http://www.wias-berlin.de/publications/reports/22/wias_reports_22.pdf

[16] O. Klein, P. Philip, J. Sprekels, K. Wilmański, Radiation- and convection-driven transient heat transfer during sublimation growth of silicon carbide single crystals, J. Crystal Growth 222 (4) (2001) 832–851.

[17] O. Klein, P. Philip, Correct voltage distribution for axisymmetric sinusoidal modeling of induction heating with prescribed current, voltage, or power, IEEE Trans. Mag. 38 (3) (2002) 1519–1523.

[18] O. Klein, P. Philip, Transient conductive-radiative heat transfer: Discrete existence and uniqueness for a finite volume scheme, Math. Mod. Meth. Appl. Sci. 15 (2) (2005) 227–258.

[19] J. Geiser, O. Klein, P. Philip, Numerical simulation of heat transfer in materials with anisotropic thermal conductivity: A finite volume scheme to handle complex geometries, Preprint No. 2046 of the Institute for Mathematics and its Applications (IMA), Minneapolis, 2005; Preprint No. 1033, Weierstrass Institute for Applied Analysis and Stochastics (WIAS), Berlin, 2005, submitted. Available at http://www.ima.umn.edu/preprints/may2005/2046.pdf

[20] J. Geiser, O. Klein, P. Philip, WIAS-HiTNIHS: Software-tool for simulation in sublimation growth for sic single crystal: Application and methods, in Proceedings of the International Congress of Nanotechnology, San Francisco, November 7-10, 2004. Available at http://www.ianano.org/Proceeding/Geiser.pdf

[21] F. Dupret, P. Nicodéme, Y. Ryckmans, P. Wouters, M.J. Crochet, Global modelling of heat transfer in crystal growth furnaces, Intern. J. Heat Mass Transfer 33 (9) (1990) 1849–1871.

[22] J. Fuhrmann, T. Koprucki, H. Langmach, pdelib: An open modular tool box for the numerical solution of partial differential equations. Design patterns, in: W. Hackbusch, G. Wittum (Eds.), Proceedings of the 14th GAMM Seminar on Concepts of Numerical Software, Kiel, January 23–25, 1998, University of Kiel, Kiel, Germany, 2001.

[23] J. Shewchuk, Triangle: Engineering a 2D quality mesh generator and delaunay triangulator, pp. 124–133 in: First Workshop on Applied Computational Geometry (Philadelphia, Pennsylvania), ACM, 1996.

[24] O. Schenk, K. Gärtner, W. Fichtner, Scalable parallel sparse factorization with left-strategy on shared memory multiprocessor, BIT 40 (1) (2000) 158–176.

[25] O. Schenk, K. Gärtner, Solving unsymmetric sparse systems of linear equations with PARDISO, Journal of Future Generation Computer Systems 20 (3) (2004) 475–487.

[26] O. Klein, P. Philip, Transient numerical investigation of induction heating during sublimation growth of silicon carbide single crystals, J. Crystal Growth 247 (1–2) (2003) 219–235.

[27] O. Klein, P. Philip, Transient temperature phenomena during sublimation growth of silicon carbide single crystals, J. Crystal Growth 249 (3–4) (2003) 514–522.

[28] R. Madar, J. Camassel, E. Blanquet (Eds.), Silicon Carbide and Related Materials ICSCRM, Lyon, France, October 5–10, 2003, Vol. 457–460, Part II of Materials Science Forum, Trans Tech Publications Ltd, 2004.